

# FastInstShadow: A Simple Query-Based Model for Instance Shadow Detection

Takeru Inoue<sup>1</sup> Ryusuke Miyamoto<sup>2</sup>

<sup>1</sup>Department of Computer Science, Graduate School of Science and Technology, Meiji University, Japan

<sup>2</sup>Department of Computer Science, School of Science and Technology Meiji University, Japan

{takeru, miya}@cs.meiji.ac.jp

## Abstract

*Instance shadow detection is the task of detecting pairs of shadows and objects, where existing methods first detect shadows and objects independently, then associate them. This paper introduces FastInstShadow, a method that enhances detection accuracy through a query-based architecture featuring an association transformer decoder with two dual-path transformer decoders to assess relationships between shadows and objects during detection. Experimental results using the SOBA dataset showed that the proposed method outperforms all existing methods across all criteria. This method makes real-time processing feasible for moderate-resolution images with better accuracy than SSISv2, the most accurate existing method. Our code is available at <https://github.com/wlotkr/FastInstShadow>.*

## 1. Introduction

Instance shadow detection methods detect shadows and their corresponding objects as pixel-wise class labels and identifies pairs between them. This is an essential process for various applications. For example, in photo editing, shadow detection allows manipulation of unified objects and their associated shadows, improving flexibility in editing operations such as deletion, scaling, and translation [40, 42, 45]. Some image generation tasks, including shadow removal, shadow generation, and object compositing, require assistance from instance shadow detection methods. A majority of shadow removal [11, 12] methods require the shadow masks as input, which can be easily obtained through instance shadow detection methods. Shadow generation [17, 27, 34] also needs the assistance from instance shadow detection methods because their accuracy can be improved by using binary masks of background objects and associated shadows as clues. Instance shadow detection methods are also effectively utilized in both the creation of the DESOBAv2 [27] dataset for shadow generation, and datasets for realistic object placement with shadow ef-

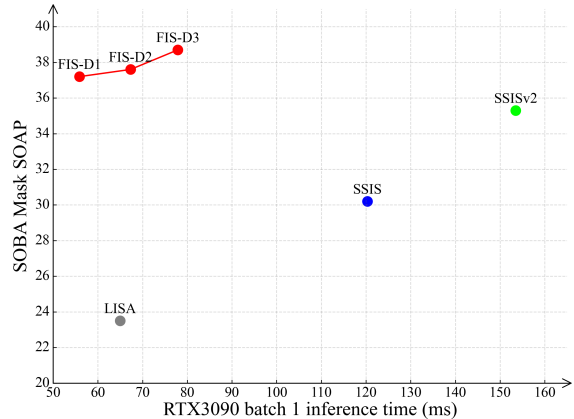


Figure 1. **Speed-performance trade-off on SOBA-testing.** Our FastInstShadow (FIS) is a scalable framework where the lightweight variant, FIS-D1, outperforms all existing methods in terms of both speed and accuracy on  $SOAP_{segm}$  [40]. The larger-scale variants, FIS-D2 and FIS-D3, achieve further accuracy improvements.

fects [3]. This emphasizes the importance of associating shadows with corresponding objects. Therefore, advances in instance shadow detection will also contribute to several types of vision tasks such as image generation, one of the hottest tasks since the rise of diffusion models [16, 32].

Existing instance shadow detection methods [40–42] attempt to solve this task through a two-stage approach: individual pixel-wise detection of shadows and objects, and pairing detected shadows with their corresponding detected objects. These methods extend instance segmentation models by incorporating pairing processes: detection is performed by an instance segmentation model, and pairing is done by an incorporated process.

Considering the current approaches to instance shadow detection, the detection and pairing accuracy strongly depends on the instance segmentation model and extended pairing process, respectively. However, despite recent attention in instance segmentation focusing on query-based methods due to their non-maximum suppression (NMS)-

free simple pipeline and high detection accuracy, no methods have yet incorporated query-based models into instance shadow detection methods. Additionally, treating detection and pairing as separate processes complicates the inference pipeline and potentially misses opportunities to learn mutual relationships of shadows and objects.

To overcome issues with existing instance shadow detection methods, this paper proposes a novel method named FastInstShadow (FIS) with sufficient accuracy and processing speed for practical applications. FIS is based on FastInst [13], a query-based instance segmentation method that delivers real-time performance and high accuracy through a simple architecture. Our key innovation is designing queries that directly aggregate shadow and object features, enabling the model to learn their mutual relationships, detecting paired shadow-object instances. The query design makes it possible to remove the pairing process of shadows and objects that is indispensable for existing methods. Additionally, we incorporate two training strategies that improve accuracy without adding complexity the inference pipeline. As shown in Fig. 1, our method achieves strong performance on the SOBA-testing [40].

Our main contributions can be summarized as follows:

- We propose the first query-based model for instance shadow detection having an association transformer decoder composed of two dual-path transformer decoders [13], eliminating the pairing processes that have been indispensable for instance shadow detection methods.
- We designed shadow direction learning and box-aware mask loss processes to improve the accuracy of instance shadow detection.
- Despite its simple architecture, our method is significantly more accurate than state-of-the-art(SOTA) methods.
- Inference speed is drastically improved, reaching more than 30 frames per second(fps) for images with moderate resolutions, with higher accuracy than SOTA methods.

## 2. Related Work

This section explains the taxonomy of instance segmentation and instance shadow detection, which is closely related to the contribution of the proposed method.

### 2.1. Instance segmentation

Existing instance shadow detection methods are based on instance segmentation models, which are vital in detecting shadows and objects. Current instance segmentation models can be grouped into region-based methods, instance activation-based methods, and query-based methods.

**Region-based methods** first detect bounding boxes for instances and then extract region features using RoI-Pooling [31] or RoI-Align [14] for pixel-wise detection

[2, 5, 20, 21, 28]. As a pioneering work, Mask R-CNN [14] extends Faster R-CNN [31] by adding a mask branch for pixel-wise detection.

**Instance activation-based methods** represent instances by semantically meaningful pixels and perform pixel-wise detection using the features of these pixels [1, 6, 8, 23, 43, 44, 46]. For example, CondInst [36] extends FCOS [35] by predicting mask embedding vectors for dynamic convolution for pixel-wise detection.

**Query-based methods** represent instances as queries and perform pixel-wise detection through transformer decoders [7, 9, 19, 24, 25]. Recent attention in instance segmentation has focused on query-based methods due to their simple, NMS-free pipelines and high accuracy. While early query-based methods were limited by slow inference speeds, FastInst [13] achieves real-time performance through architectural refinements.

### 2.2. Instance shadow detection

We present details of both existing instance shadow detection stages: the first utilizes instance segmentation and the second implements the pairing process.

**Region-based methods** were first introduced to instance shadow detection through LISA [40], an extension of Mask R-CNN [14] featuring a separate branch for detecting integrated regions for each shadow-object pair and a heuristic pairing algorithm. The main branch inherited from Mask R-CNN detects individual shadows and objects, then a heuristic pairing algorithm associates them. The pairing algorithm selects candidate pairs when the distance between detected shadows and objects is below an empirical threshold. The algorithm finalizes pairs by evaluating the IoU scores between the merged regions of candidate pairs and the detections from the separate branch.

**Instance activation-based methods** were introduced to instance shadow detection through SSIS[41] and SSISv2[42]. These methods extend CondInst with a separate head for detecting associated instances and a heuristic pairing algorithm. The main head inherited from CondInst detects individual shadows and objects, while the separate head detects instances paired with the main head’s instances. Thus, these methods detect shadows and objects as pairs; however, the detection accuracy of the separate head is lower than that of the main head. Therefore, these methods also employ a heuristic pairing algorithm to pair shadow and object detections from the main head. However, the relationships between shadow and objects detected by the main head are not considered in the detection stage.

Region-based and instance activation-based methods represent instances using bounding boxes and semantically meaningful pixels, respectively. As, these methods cannot address shadow and object dependencies, we introduce a query-based instance shadow detection method that

has gained popularity in the field of instance segmentation which can treat relationships between shadows and objects appropriately.

### 2.3. FastInst Architecture

FastInst [13] follows the meta-architecture of Mask2Former [7] and integrates three key innovations:

(i) **Instance activation-guided queries** dynamically select pixel embeddings with high semantics from feature maps as initial queries, enriching embedding information. This reduces the iteration update burden of the transformer decoder.

(ii) **Dual-path update strategy** alternately updates query and pixel features, enhancing the representation ability of pixel features. This saves us from the heavy pixel decoder design and reduces dependence on the number of decoder layers.

(iii) **Ground truth mask-guided learning** replaces the mask used in the standard masked attention with the last layer bipartite matched ground truth mask. This allows each query to see the whole region of its predicted target instances during training.

These innovations enable FastInst to achieve high accuracy and real-time instance segmentation. Similarly, we leverage these innovations in our method to achieve high accuracy and real-time instance shadow detection.

## 3. Methods

In this section, we present our FIS method, based on FastInst. We describe two strategies employed to train this architecture: shadow direction learning and box-aware mask loss.

### 3.1. Overall architecture

Figure 2 illustrates the architecture of FIS. Our model first extracts three feature maps  $C_3$ ,  $C_4$  and  $C_5$ , where resolutions are  $1/8$ ,  $1/16$  and  $1/32$  of the input image  $I \in \mathbb{R}^{H \times W \times 3}$ , respectively, using ResNet-50-d [15] with deformable convolutions [49] as a backbone. Three feature maps are projected to 256 channel maps by a  $1 \times 1$  convolutional layer. PPM-FPN [8], as a pixel decoder, accepts these feature maps as input and then outputs multi-scale feature maps  $E_3$ ,  $E_4$  and  $E_5$ . Subsequently,  $N_a$  instance activation-guided queries [13] select pixel embeddings with higher object semantics. These queries are concatenated with  $N_b$  auxiliary learnable queries to obtain the total queries  $Q \in \mathbb{R}^{N \times 256}$ , where  $N = N_a + N_b$ . Additionally, the high-resolution pixel feature  $E_3$  is flattened to produce object pixel features  $X_o \in \mathbb{R}^{L \times 256}$  and shadow pixel features  $X_s \in \mathbb{R}^{L \times 256}$ , where  $L = H/8 \times W/8$ . The association transformer decoder then accepts these features as input for performing pixel-wise detection of shadows and objects as pairs.

### 3.2. Association transformer decoder

The association transformer decoder consists of two dual-path transformer decoders [13] connected sequentially. The two dual-path transformer decoders focus on object and shadow features, respectively. When queries  $Q$ , object pixel features  $X_o$ , and shadow pixel features  $X_s$  are input to the association transformer decoder, positional embeddings are added to these features. Next, queries  $Q$  and object pixel features  $X_o$  are input to the first dual-path transformer decoder. Here, object pixel features  $X_o$  are updated through the cross-attention layer on queries  $Q$  and the feedforward layer. Then, queries  $Q$  are updated through masked attention, self-attention, and the feedforward layer. Masked attention aggregates object features into queries  $Q$  using predicted object masks from the previous layer.

Furthermore, updated queries  $Q$  and shadow pixel features  $X_s$  are input to the second dual-path transformer decoder. Similar to the first decoder, shadow pixel features  $X_s$  are updated through the cross-attention layer on updated queries  $Q$  and the feedforward layer. At this stage, queries  $Q$  already contain object features, assisting the transformer decoder in detecting shadows that correspond to the objects. Then, similar to the first decoder, queries  $Q$  are updated through masked attention, self-attention and feedforward layer. Masked attention aggregates shadow features into queries  $Q$  using predicted shadow masks from the previous layer. The association transformer decoder takes object pixel features  $X_o$ , shadow pixel features  $X_s$ , and queries  $Q$  as input and outputs updated object pixel features  $X'$ , shadow pixel features  $X'_s$ , and queries  $Q'$ . These updated features are then used as input to the next Association Transformer decoder. By repeatedly employing the association transformer decoder, queries  $Q$  aggregate object and shadow features, capturing their mutual relationships.

During inference, a three-layer MLP is applied to refined queries  $Q$  to obtain mask embeddings. A linear projection is applied to refined object pixel features  $X_o$  and shadow pixel features  $X_s$  to obtain object and shadow mask features, respectively. Then, object and shadow masks for each query are obtained by multiplying mask embeddings with each mask feature.

### 3.3. Training strategies

#### 3.3.1. Shadow direction learning

In the FIS architecture, the association transformer decoder learns the mutual relationships between shadows and objects. To further facilitate relation learning, we implement a directional learning strategy from objects to shadows. In this strategy, an offset vector map is first generated by reducing the channel dimension of the output from the pixel decoder  $E_3$  through a  $3 \times 3$  convolutional layer. This offset vector map contains two channels representing  $x$  and  $y$  coordinates. The offset vector map is denoted as

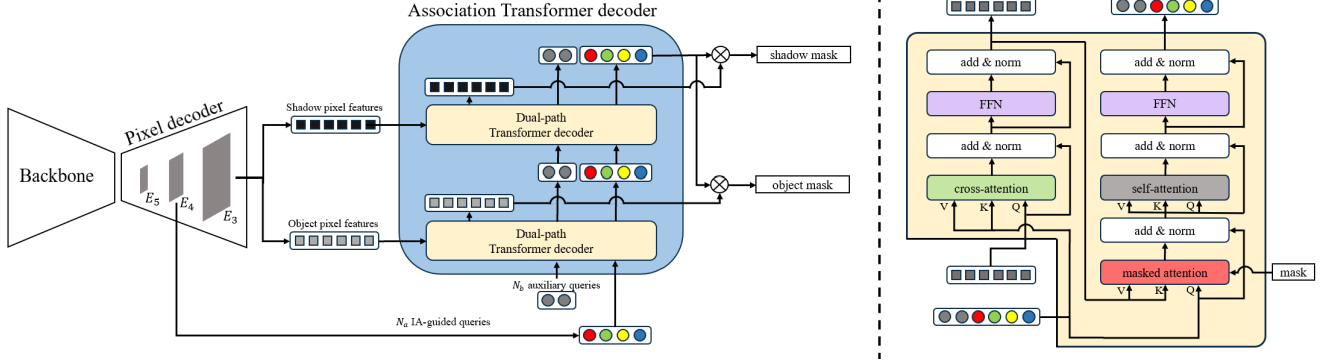


Figure 2. **FastInstShadow(FIS) architecture.** The left side of the figure illustrates the overall architecture, while the right side details the dual-path transformer decoder [13]. FIS consists of three components: a backbone network and a pixel decoder, both inherited from FastInst [13], along with our novel association transformer decoder. Furthermore, object and shadow pixel features, obtained by flattening the feature map  $E_3$ , along with queries designed similar to FastInst, are input into the association transformer decoder. The association transformer decoder consists of two dual-path Transformer decoders: the first processes object pixel features to capture object characteristics and the second processes shadow pixel features to capture shadow characteristics. This design enables the model to detect shadows and objects as paired instances while considering their mutual relationships.

$V \in \mathbb{R}^{H' \times W' \times 2}$ , where  $H' = H/8$  and  $W' = W/8$ . Subsequently, center coordinates of object masks obtained by the association transformer decoder are computed and the corresponding offset vectors are extracted from the offset vector map  $V$  at these coordinates. The model is then trained to match the sum of each query’s object mask center coordinates and offset vector with the shadow mask’s ground-truth center coordinates.

Our proposed shadow direction loss  $\mathcal{L}_d$  is defined as:

$$\mathcal{L}_d = \begin{cases} \lambda_d(0.5(\theta^p - \theta^g)^2/\beta), & \text{if } |\theta^p - \theta^g| < \beta \\ \lambda_d(|\theta^p - \theta^g| - 0.5 \cdot \beta), & \text{otherwise,} \end{cases} \quad (1)$$

where  $\lambda_d$  is the loss weight,  $\beta$  is a hyperparameter, and  $\theta^p$  and  $\theta^g$  are the predicted and ground-truth coordinates of the shadow, respectively. The smooth  $\mathcal{L}_1$  loss [10] is used as shadow direction loss.

This strategy for learning bidirectional relationships between shadows and objects has also been employed in LISA [40], SSIS [41], and SSISv2 [42]. However, while SSIS and SSISv2 transform inferred coordinates into a map and use it as input to the mask head, our method does not utilize inferred coordinates for shadow and object detection, similar to LISA. This approach allows us to maintain a simple pipeline during inference while improving accuracy.

### 3.3.2. Box-aware mask loss

Our architecture does not include a mechanism for predicting bounding boxes of shadows and objects, unlike existing instance shadow methods [40–42]. Consequently, generated masks may not consider their bounding boxes, leading to false positive detections that deviate significantly from ground truth regions. In particular, shadow detec-

tion is challenging due to similar shadow textures regardless of which objects cast them, as well as irregular shapes caused by lighting conditions, making these masks prone to such deviant false positive detections. Thus, we introduce a reweighting strategy in binary mask cross-entropy loss.

Our proposed loss function is defined as:

$$\mathcal{L}_{ce} = -\frac{1}{K} \sum_{i=1}^K w_i [y_i \cdot \log(p_i) + (1 - y_i) \cdot \log(1 - p_i)]$$

$$w_i = \begin{cases} \alpha & \text{if point } i \text{ is outside the AABB} \\ & \text{and } p_i > 0.5 \text{ where } y_i = 0 \\ 1 & \text{otherwise} \end{cases} \quad (2)$$

In our method, similar to [7, 13], the mask loss is computed using  $K$  randomly sampled points.  $y_i$ ,  $p_i$  and  $w_i$  represent the target label, the predicted probability and the weight at the sampled point  $i$ , respectively. This loss function assigns a larger value to  $w_i$  when point  $i$  is outside the axis-aligned bounding box (AABB) of the corresponding ground truth mask and incorrectly predicted as positive. This weighting scheme penalizes deviant false positive pixels, thereby suppressing such detections. However, applying this weighting scheme in early training phase can result in inaccurate training. Therefore, we only apply this loss function after  $N$  epochs of training, using the conventional loss function with  $w_i = 1$  until epoch  $N$ .

### 3.3.3. Overall loss function

The overall loss function for FIS can be expressed as:

$$\mathcal{L} = \mathcal{L}_{\text{IA-q}} + \mathcal{L}_{\text{pred}} + \mathcal{L}'_{\text{pred}} + \mathcal{L}_d, \quad (3)$$

where  $\mathcal{L}_{\text{IA-q}}$ ,  $\mathcal{L}_{\text{pred}}$  and  $\mathcal{L}'_{\text{pred}}$  are instance activation loss, prediction loss and GT mask-guided loss, respectively.  $\mathcal{L}_d$  is

Network	fps	$SOAP_{segm}$	$SOAP_{bbox}$	Assoc. $AP_{segm}$	Assoc. $AP_{bbox}$	Inst. $AP_{segm}$	Inst. $AP_{bbox}$
LISA [40]	15.38	23.5	21.9	40.9	48.4	39.2	37.6
SSIS [41]	8.31	30.2	27.1	52.2	59.6	43.4	41.3
SSISv2 [42]	6.51	35.3	29.0	59.2	63.1	50.2	44.4
FIS-D1	<b>17.89</b>	37.2	33.3	63.0	62.3	52.4	50.2
FIS-D2	14.89	37.6	33.2	63.3	63.8	53.7	51.6
FIS-D3	12.84	<b>38.7</b>	<b>35.6</b>	<b>63.8</b>	<b>65.9</b>	<b>53.8</b>	<b>53.0</b>

Table 1. **Instance shadow detection on SOBA-testing.** Our FIS demonstrates a favorable trade-off between scaling and performance: while larger variants exhibit slower inference speeds, they achieve progressively higher accuracy. FIS-D1 surpasses SOTA methods across most evaluation metrics while achieving the fastest inference speed. Furthermore, FIS-D3 outperforms all existing approaches across all metrics, establishing new enhanced SOTA performance. Inference speed was measured using the entire SOBA-testing.

Network	$SOAP_{segm}$	$SOAP_{bbox}$	Assoc. $AP_{segm}$	Assoc. $AP_{bbox}$	Inst. $AP_{segm}$	Inst. $AP_{bbox}$
LISA [40]	10.4	10.1	20.7	25.8	23.8	24.3
SSIS [41]	12.7	12.8	28.4	32.6	25.6	26.2
SSISv2 [42]	17.7	15.1	34.6	37.3	31.0	28.4
FIS-D1	18.9	14.1	36.1	34.6	33.5	30.0
FIS-D2	20.6	16.7	38.5	35.9	35.6	32.7
FIS-D3	<b>21.0</b>	<b>17.5</b>	<b>40.0</b>	<b>38.8</b>	<b>36.3</b>	<b>33.9</b>

Table 2. **Instance shadow detection on SOBA-challenge.** SOBA-challenge [42] is a dataset for evaluating detection performance in complex scenarios. FIS-D3 establishes new enhanced SOTA performance even on this test set.

shadow direction loss shown as Eq. (1). The Hungarian algorithm [22] is employed to establish an optimal bipartite matching between predictions and the ground truth set similar to [4, 13, 33]. Since detecting objects is more accurate than shadows, this algorithm is performed considering only object masks, using the same costs as [13].

**Instance activation loss**  $\mathcal{L}_{IA-q}$  is defined as:

$$\mathcal{L}_{IA-q} = \lambda_{cls-q} \mathcal{L}_{cls-q}, \quad (4)$$

where  $\lambda_{cls-q}$  is the loss weight and  $\mathcal{L}_{cls-q}$  denotes the cross-entropy loss.  $\mathcal{L}_{cls-q}$  is calculated for the probabilities obtained from the auxiliary classification head added on top of the feature map  $E_4$ . Since each query in our model contains paired shadow-object features,  $\mathcal{L}_{cls-q}$  is calculated based on whether a query is assigned to a shadow-object pair.

**Prediction loss.** The  $\mathcal{L}_{pred}$  is defined as:

$$\mathcal{L}_{pred} = \sum_{i=0}^D (\lambda_{ce} \mathcal{L}_{o\ ce}^i + \lambda_{dice} \mathcal{L}_{o\ dice}^i + \lambda_{ce} \mathcal{L}_{s\ ce}^i + \lambda_{dice} \mathcal{L}_{s\ dice}^i) + \lambda_{cls} \mathcal{L}_{cls}^i \quad (5)$$

We extend the prediction loss from [7, 13] to calculate loss for shadow masks, where  $D$  denotes the number of transformer decoder layers,  $i = 0$  represents the prediction loss for IA-guided queries. Here,  $\mathcal{L}_{o\ ce}$  and  $\mathcal{L}_{o\ dice}$  denote the box-aware mask loss defined in Eq. (2) and the Dice loss [30] for object masks, respectively. Similarly,  $\mathcal{L}_{s\ ce}$  and  $\mathcal{L}_{s\ dice}$  denote the box-aware mask loss and Dice loss for shadow masks, respectively.  $\lambda_{ce}$ ,  $\lambda_{dice}$  and  $\lambda_{cls}$  are loss

weights.  $\mathcal{L}_{cls}$  is calculated based on whether a query is assigned to a shadow-object pair, similar to  $\mathcal{L}_{cls-q}$ .

**GT mask-guided loss.**  $\mathcal{L}'_{pred}$  is similar to Eq. (5). The only differences are that it applies mask-guided learning [13] while skipping calculation of the zeroth layer loss.

## 4. Experiments

This section compares the performance of FIS using the SOBA [40–42] dataset with other SOTA instance shadow detection methods. In the evaluation, relations between the inference speed and the detection accuracy are shown while changing the number of association transformer decoder layers implemented in FIS. FIS-D $\Gamma$  represents FIS with  $\Gamma$  association transformer decoder layers. In addition to these evaluations, we also demonstrate the effectiveness of the proposed training strategy composed of shadow direction learning and box-aware mask loss.

### 4.1. Implementation details

We used the AdamW [29] optimizer with a learning rate of  $1 \times 10^{-4}$  and a weight decay of 0.05. There is a 1,000 iterations linear warmup and a cosine decaying schedule afterward. Our model was trained for 100 epochs with a batch size of 4. We employed the same data augmentation method as SSISv2 [42]. We initialized FIS weights by transferring the applicable portions from FastInst pretrained on the COCO [26] dataset. To avoid data leakage, we excluded images from the COCO dataset that overlapped with the SOBA-testing for pretraining. The loss weights  $\lambda_{cls-q}$ ,  $\lambda_{cls}$ ,

	+ shadow direction learning	+ box -aware mask loss	$SOAP_{segm}$	$SOAP_{bbox}$	Assoc. $AP_{segm}$	Assoc. $AP_{nbbox}$	Inst. $AP_{segm}$	Inst. $AP_{bbox}$
FIS-D3			37.8	32.5	63.1	62.1	53.1	49.4
	✓		38.1	32.8	63.5	62.2	<b>53.8</b>	50.6
		✓	37.2	33.3	62.9	62.4	53.4	51.2
	✓	✓	<b>38.7</b>	<b>35.6</b>	<b>63.8</b>	<b>65.9</b>	<b>53.8</b>	<b>53.0</b>

Table 3. **Training strategy analysis on SOBA-testing.** The results demonstrate that integrating the shadow direction learning strategy improves  $SOAP_{segm}$  and  $SOAP_{bbox}$ . In addition, the box-aware mask loss particularly improves  $SOAP_{bbox}$ . By introducing both shadow direction learning and box-aware mask loss, we achieve the highest accuracy in all metrics.

	+ shadow direction learning	+ box -aware mask loss	$SOAP_{segm}$	$SOAP_{bbox}$	Assoc. $AP_{segm}$	Assoc. $AP_{bbox}$	Inst. $AP_{segm}$	Inst. $AP_{bbox}$
FIS-D3			18.4	14.0	36.1	32.1	33.6	29.1
	✓		20.5	15.6	38.0	34.8	35.3	31.2
		✓	19.7	16.2	38.6	35.6	35.4	32.9
	✓	✓	<b>21.0</b>	<b>17.5</b>	<b>40.0</b>	<b>38.8</b>	<b>36.3</b>	<b>33.9</b>

Table 4. **Training strategy analysis on SOBA-challenge.** The effectiveness of the two strategies is also demonstrated even on this test set.

$\lambda_{ce}$ ,  $\lambda_{dice}$  and  $\lambda_d$  were set to 20.0, 2.0, 5.0, 5.0 and 0.1, respectively. For shadow direction learning,  $\beta$  was set to 0.5. For box-aware mask loss,  $N$  and  $\alpha$  were set to 75 and 50, respectively. Following the evaluation protocol of existing methods [40–42], we reported SOAP [40], instance AP, and association AP on both SOBA-testing and SOBA-challenge for the model trained on SOBA-training. Since FIS does not have a mechanism to detect bounding boxes, the  $AP_{bbox}$  evaluation of FIS used the AABB of the generated mask. We also measured the inference speed of the shadow and object masks as fps. All inference speed measurements were conducted on an RTX3090 GPU with a batch size of 1. Unless specified, we resized input images to a shorter edge of 800 pixels and ensured a maximum length of 1,333 pixels during testing, similar to existing methods [40–42].

## 4.2. Comparison with state-of-the-art methods

We compared our proposed FIS with SOTA methods. The comparative results for SOBA-testing and SOBA-challenge are presented in Tab. 1 and 2, respectively. All FIS series surpassed SOTA methods in instance AP, which evaluates individual shadow and object detection accuracy. This demonstrates that our simple architectural extension preserves the high detection capability of the base FastInst model. Almost FIS series also surpassed SOTA methods in SOAP, which evaluates shadow-object detection accuracy and correct pairing performance. Existing instance shadow detection methods employ additional detection and heuristic pairing algorithms for pairing, whereas our method does not use pairing process, detecting shadows and objects as pairs. These SOAP results demonstrate the effectiveness of

our paired detection method. Almost FIS series surpassed SOTA methods in association AP, which evaluates detection of integrated regions for each shadow-object pair. Remarkably, FIS-D3 exceeded SOTA performance across all metrics on SOBA-testing and SOBA-challenge.

As shown in the second column of Tab. 1, FIS series demonstrates high inference speed. Remarkably, FIS-D1 achieves higher inference speed than all existing methods. This performance advantage is a result of our simple extension to the FastInst, real-time instance segmentation model.

Next, we provide visual comparison results in Fig. 3, where (a) shows input images (b),(c),(d),(e) show the results produced using LISA [40], SSIS [41], SSISv2 [42] and FIS-D3, respectively. The results show that (i) FIS-D3 can detect shadows and objects more accurately, as shown in the first five rows and (ii) FIS-D3 can discover more shadow-object association pairs, even for small objects, as shown in the last three rows.

## 4.3. Additional analysis

After introducing two training strategies, we then verified their effectiveness. Additionally, we provide a more detailed analysis of their instance AP and fps.

### Analysis of training strategies

We evaluated the effectiveness of two proposed training strategies: shadow direction learning and box-aware mask loss. Quantitative comparisons on SOBA-testing and SOBA-challenge are shown in Tab. 3 and 4, respectively. The results demonstrate that integrating the shadow direction learning strategy improves all criteria. In addition, the

method	dataset	AP	AP <sub>S</sub>	AP <sub>M</sub>	AP <sub>L</sub>
CondInst	COCO	39.1	<b>21.5</b>	41.7	50.9
FastInst-D3	test-dev	<b>40.5</b>	11.9	<b>57.9</b>	<b>76.7</b>
SSISv2	SOBA	50.0	17.4	48.8	72.4
FIS-D3	-testing	<b>53.8</b>	<b>21.1</b>	<b>52.5</b>	<b>76.1</b>
SSISv2	SOBA	30.8	7.9	26.4	43.9
FIS-D3	-challenge	<b>36.3</b>	<b>11.7</b>	<b>33.0</b>	<b>48.8</b>

Table 5. **Details of instance AP.** FastInst-D3 [13] which is the base model of FIS-D3 demonstrated lower detection accuracy for small instances compared to CondInst [36] which is the base model of SSISv2. However, when comparing FIS-D3 and SSISv2, FIS-D3 achieved higher detection accuracy for small instances. Since the original SSISv2 study [42] did not report detailed instance AP, their results were reproduced using the official pre-trained model from <https://github.com/steveuwongv/SSIS>.

box-aware mask loss improves box-based detection metrics. This reduces false positive detections that significantly deviate from ground truth regions, obtaining appropriate AABB and improving box-based detection metrics. Introducing both shadow direction learning and box-aware mask loss result in the highest accuracy across all metrics on SOBA-testing and SOBA-challenge. Consequently, it is demonstrated that our two strategies contribute to accuracy improvement.

### Analysis of instance AP

We conducted a detailed instance AP comparison between FIS and SSISv2, the current SOTA method. We present the instance segmentation accuracy on the COCO [26] dataset for CondInst, which is the base model of SSISv2, and FastInst, which is the base model of FIS, in the second and third rows of Tab. 5. This table shows that FastInst faces a limitation with low detection accuracy for small instances. However, it is demonstrated that FIS-D3 is more accurate than SSISv2 for small instance detection on the SOBA dataset, as shown in the last four rows of Tab. 5.

### Analysis of real-time performance

The fps reported in Tab. 1 fails to achieve real-time requirements ( $\geq 30$  fps) due to the large inference and input image sizes. To properly assess FIS-D1’s real-time performance, this section evaluates the model using an appropriately sized inferences and input images. The SOBA-testing is composed of images from the ADE20K [47, 48], SBU [18, 37, 38], ISTD [39], and COCO [26] datasets, along with web-collected images. Notably, images collected from the web in the SOBA-testing have higher resolutions, which deviate from the standard image sizes of COCO test-dev, the benchmark for instance segmentation speed measurements. When processing such large images,

Network	fps	$SOAP_{segm}$	Assoc. $AP_{segm}$	Inst. $AP_{segm}$
SSISv2	10.76	38.3	57.80	52.26
FIS-D1	<b>32.21</b>	<b>39.3</b>	<b>60.57</b>	<b>52.27</b>

Table 6. **Instance shadow detection on a dataset excluding web-collected images from SOBA-testing.** Our FIS-D1 surpasses SOTA method in terms of mask-based detection metrics while enabling real-time processing. The result of SSISv2 [42] was reproduced using the official pretrained model. The input images of FIS-D1 were resized to a width of 640 pixels and a maximum length of 853 pixels, while the input images of SSISv2 were resized to a width of 800 pixels and a maximum length of 1,333 pixels.

the time required to resize generated masks to their original resolutions becomes non-negligible. Therefore, we validated FIS-D1’s real-time performance on a dataset excluding web-collected images from SOBA-testing. The dataset’s average image size is  $453 \times 584$  pixels, similar to COCO test-dev’s average size of  $484 \times 574$  pixels. When inputting images to our model, we resized them to a shorter edge of 640 pixels and ensured a maximum length of 853 pixels. The resulting inference speed and accuracy are presented in Tab. 6. Here, FIS-D1 achieves real-time requirements and higher accuracy compared to SSISv2, the most accurate existing method.

## 5. Conclusion

This paper proposed a novel method for instance shadow detection named FastInstShadow (FIS), which adopts a query-based method to treat relationships between shadow and object features appropriately during the detection process though existing methods detect shadows and objects independently. The primary innovation of FIS is association transformer decoder, composed of two dual-path transformer decoders: one to process object pixel features and the other to process shadow pixel features. In addition to the architectural modifications, shadow direction learning and box-aware mask loss were designed to improve instance shadow detection accuracy. Our FIS has the capability to perform instance-shadow detection without the pairing process of shadows and objects that has been indispensable to existing methods.

Experimental results using the SOBA datasets showed that detection accuracy and processing speed drastically improved: FIS-D3 achieved the highest accuracy across all criteria, and FIS-D1 achieved the highest processing speed among all existing methods. The processing speed of FIS-D1 reached more than 30 fps for input images with moderate resolutions while maintaining better accuracy than SSISv2, the most accurate existing method.

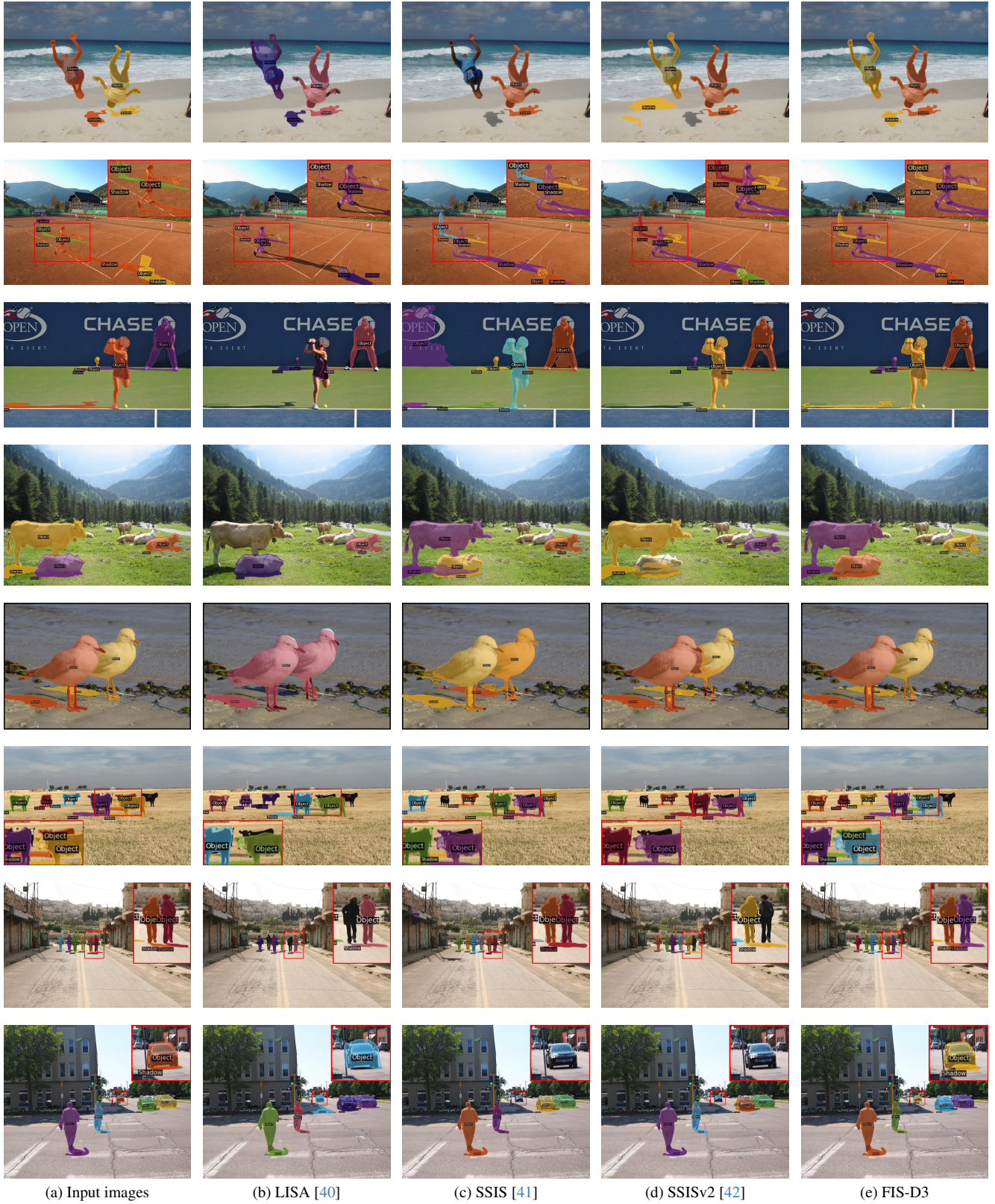


Figure 3. **Visual comparison of some detections.** These results produced by various methods (b)-(e) on images (a) in the SOBA-testing or SOBA-challenge set. The regions in red boxes are zoomed for better visualization.

## References

- [1] Daniel Bolya, Chong Zhou, Fanyi Xiao, and Yong Jae Lee. YOLACT++ better real-time instance segmentation. *IEEE Trans. Pattern Analysis and Machine Intelligence*, 44(2): 1108–1121, 2022. 2
- [2] Zhaowei Cai and Nuno Vasconcelos. Cascade R-CNN: High quality object detection and instance segmentation. *IEEE Trans. Pattern Analysis and Machine Intelligence*, 43(5): 1483–1498, 2021. 2
- [3] Gemma Canet Tarrés, Zhe Lin, Zhifei Zhang, Jianming Zhang, Yizhi Song, Dan Ruta, Andrew Gilbert, John Collosse, and Soo Ye Kim. Thinking outside the bbox: Unconstrained generative object compositing. In *Proc. European Conference on Computer Vision*, pages 476–495, 2024. 1
- [4] Nicolas Carion, Francisco Massa, Gabriel Synnaeve, Nicolas Usunier, Alexander Kirillov, and Sergey Zagoruyko. End-to-end object detection with transformers. In *Proc. European Conference on Computer Vision*, pages 213–219, 2020. 5
- [5] Kai Chen, Jiangmiao Pang, Jiaqi Wang, Yu Xiong, Xiaoxiao Li, Shuyang Sun, Wansen Feng, Ziwei Liu, Jianping Shi, Wanli Ouyang, Chen Change Loy, and Dahua Lin. Hybrid task cascade for instance segmentation. In *Proc. IEEE Conf. on Computer Vision and Pattern Recognition*, pages 4969–4978, 2019. 2
- [6] Xinlei Chen, Ross Girshick, Kaiming He, and Piotr Dollar. TensorMask: A foundation for dense object segmentation. In *Proc. IEEE International Conference on Computer Vision*, pages 2061–2069, 2019. 2
- [7] Bowen Cheng, Ishan Misra, Alexander G. Schwing, Alexander Kirillov, and Rohit Girdhar. Masked-attention mask transformer for universal image segmentation. In *Proc. IEEE Conf. on Computer Vision and Pattern Recognition*, pages 1280–1289, 2022. 2, 3, 4, 5
- [8] Tianheng Cheng, Xinggang Wang, Shaoyu Chen, Wenqiang Zhang, Qian Zhang, Chang Huang, Zhaoxiang Zhang, and Wenyu Liu. Sparse instance activation for real-time instance segmentation. In *Proc. IEEE Conf. on Computer Vision and Pattern Recognition*, pages 4423–4432, 2022. 2, 3
- [9] Bin Dong, Fangao Zeng, Tiancai Wang, Xiangyu Zhang, and Yichen Wei. SOLQ: Segmenting objects by learning queries. In *Proc. Advances in Neural Information Processing Systems*, pages 21898–21909, 2021. 2
- [10] Ross Girshick. Fast R-CNN. In *Proc. IEEE International Conference on Computer Vision*, pages 1440–1448, 2015. 4
- [11] Lanqing Guo, Siyu Huang, Ding Liu, Hao Cheng, and Bihan Wen. ShadowFormer: Global context helps shadow removal. In *Proc. AAAI Conference on Artificial Intelligence*, pages 710–718, 2023. 1
- [12] Lanqing Guo, Chong Wang, Wenhan Yang, Siyu Huang, Yufei Wang, Hanspeter Pfister, and Bihan Wen. ShadowDiffusion: When degradation prior meets diffusion model for shadow removal. In *Proc. IEEE Conf. on Computer Vision and Pattern Recognition*, pages 14049–14058, 2023. 1
- [13] Junjie He, Pengyu Li, Yifeng Geng, and Xuansong Xie. FastInst: A simple query-based model for real-time instance segmentation. In *Proc. IEEE Conf. on Computer Vision and Pattern Recognition*, pages 23663–23672, 2023. 2, 3, 4, 5, 7
- [14] Kaiming He, Georgia Gkioxari, Piotr Dollár, and Ross Girshick. Mask R-CNN. In *Proc. IEEE International Conference on Computer Vision*, pages 2980–2988, 2017. 2
- [15] Tong He, Zhi Zhang, Hang Zhang, Zhongyue Zhang, Junyuan Xie, and Mu Li. Bag of tricks for image classification with convolutional neural networks. In *Proc. IEEE Conf. on Computer Vision and Pattern Recognition*, pages 558–567, 2019. 3
- [16] Jonathan Ho, Ajay Jain, and Pieter Abbeel. Denoising diffusion probabilistic models. In *Proc. Advances in Neural Information Processing Systems*, pages 6840–6851, 2020. 1
- [17] Yan Hong, Li Niu, and Jianfu Zhang. Shadow generation for composite image in real-world scenes. In *Proc. AAAI Conference on Artificial Intelligence*, pages 914–922, 2022. 1
- [18] Le Hou, Tomás F. Yago Vicente, Minh Hoai, and Dimitris Samaras. Large scale shadow annotation and detection using lazy annotation and stacked cnns. *IEEE Trans. Pattern Analysis and Machine Intelligence*, 43(4):1337–1351, 2021. 7
- [19] Jie Hu, Liujuan Cao, Yao Lu, Shengchuan Zhang, Yan Wang, Ke Li, Feiyue Huang, Ling Shao, and Rongrong Ji. ISTR: End-to-end instance segmentation with transformers. arXiv preprint arXiv:2105.00637, 2021. 2
- [20] Zhaojin Huang, Lichao Huang, Yongchao Gong, Chang Huang, and Xinggang Wang. Mask Scoring R-CNN. In *Proc. IEEE Conf. on Computer Vision and Pattern Recognition*, pages 6402–6411, 2019. 2
- [21] Alexander Kirillov, Yuxin Wu, Kaiming He, and Ross Girshick. PointRend: Image segmentation as rendering. In *Proc. IEEE Conf. on Computer Vision and Pattern Recognition*, pages 9796–9805, 2020. 2
- [22] Harold W Kuhn. The hungarian method for the assignment problem, 1955. 5
- [23] Youngwan Lee and Jongyoul Park. CenterMask: Real-time anchor-free instance segmentation. In *Proc. IEEE Conf. on Computer Vision and Pattern Recognition*, pages 13903–13912, 2020. 2
- [24] Feng Li, Hao Zhang, Huaizhe Xu, Shilong Liu, Lei Zhang, Lionel M. Ni, and Heung-Yeung Shum. Mask DINO: Towards a unified transformer-based framework for object detection and segmentation. In *Proc. IEEE Conf. on Computer Vision and Pattern Recognition*, pages 3041–3050, 2023. 2
- [25] Zhiqi Li, Wenhai Wang, Enze Xie, Zhiding Yu, Anima Anandkumar, Jose M. Alvarez, Ping Luo, and Tong Lu. Panoptic SegFormer: Delving deeper into panoptic segmentation with transformers. In *Proc. IEEE Conf. on Computer Vision and Pattern Recognition*, pages 1270–1279, 2022. 2
- [26] Tsung-Yi Lin, Michael Maire, Serge Belongie, James Hays, Pietro Perona, Deva Ramanan, Piotr Dollár, and C Lawrence Zitnick. Microsoft COCO: Common objects in context. In *Proc. European Conference on Computer Vision*, pages 740–755, 2014. 5, 7
- [27] Qingyang Liu, Junqi You, Jianting Wang, Xinhao Tao, Bo Zhang, and Li Niu. Shadow generation for composite image using diffusion model. In *Proc. IEEE Conf. on Computer Vision and Pattern Recognition*, pages 8121–8130, 2024. 1

- [28] Shu Liu, Lu Qi, Haifang Qin, Jianping Shi, and Jiaya Jia. Path aggregation network for instance segmentation. In *Proc. IEEE Conf. on Computer Vision and Pattern Recognition*, pages 8759–8768, 2018. [2](#)
- [29] Ilya Loshchilov and Frank Hutter. Decoupled weight decay regularization. In *Proc. International Conference on Learning Representations*, 2019. [5](#)
- [30] Fausto Milletari, Nassir Navab, and Seyed-Ahmad Ahmadi. V-Net: Fully convolutional neural networks for volumetric medical image segmentation. In *Proc. International Conference on 3D Vision*, pages 565–571, 2016. [5](#)
- [31] Shaoqing Ren, Kaiming He, Ross Girshick, and Jian Sun. Faster R-CNN: Towards real-time object detection with region proposal networks. In *Proc. Advances in Neural Information Processing Systems*, pages 91–99, 2015. [2](#)
- [32] Jascha Sohl-Dickstein, Eric A. Weiss, Niru Maheswaranathan, and Surya Ganguli. Deep unsupervised learning using nonequilibrium thermodynamics. In *Proc. International Conference on Machine Learning*, pages 2256–2265, 2015. [1](#)
- [33] Russell Stewart, Mykhaylo Andriluka, and Andrew Y. Ng. End-to-end people detection in crowded scenes. In *Proc. IEEE Conf. on Computer Vision and Pattern Recognition*, pages 2325–2333, 2016. [5](#)
- [34] Xinhao Tao, Junyan Cao, Yan Hong, and Li Niu. Shadow generation with decomposed mask prediction and attentive shadow filling. In *Proc. AAAI Conference on Artificial Intelligence*, pages 5198–5206, 2024. [1](#)
- [35] Zhi Tian, Chunhua Shen, Hao Chen, and Tong He. FCOS: Fully convolutional one-stage object detection. In *Proc. IEEE International Conference on Computer Vision*, pages 9626–9635, 2019. [2](#)
- [36] Zhi Tian, Chunhua Shen, and Hao Chen. Conditional convolutions for instance segmentation. In *Proc. European Conference on Computer Vision*, pages 282–298, 2020. [2](#), [7](#)
- [37] Tomás F. Yago Vicente, Minh Hoai, and Dimitris Samaras. Noisy label recovery for shadow detection in unfamiliar domains. In *Proc. IEEE Conf. on Computer Vision and Pattern Recognition*, pages 3783–3792, 2016. [7](#)
- [38] T. F. Y. Vicente, Le Hou, Chen-Ping Yu, Minh Hoai, and Dimitris Samaras. Large-scale training of shadow detectors with noisily-annotated shadow examples. In *Proc. European Conference on Computer Vision*, pages 816–832, 2016. [7](#)
- [39] Jifeng Wang, Xiang Li, and Jian Yang. Stacked conditional generative adversarial networks for jointly learning shadow detection and shadow removal. In *Proc. IEEE Conf. on Computer Vision and Pattern Recognition*, pages 1788–1797, 2018. [7](#)
- [40] Tianyu Wang, Xiaowei Hu, Qiong Wang, Pheng-Ann Heng, and Chi-Wing Fu. Instance shadow detection. In *Proc. IEEE Conf. on Computer Vision and Pattern Recognition*, pages 1877–1886, 2020. [1](#), [2](#), [4](#), [5](#), [6](#), [8](#)
- [41] Tianyu Wang, Xiaowei Hu, Chi-Wing Fu, and Pheng-Ann Heng. Single-stage instance shadow detection with bidirectional relation learning. In *Proc. IEEE Conf. on Computer Vision and Pattern Recognition*, pages 1–11, 2021. [2](#), [4](#), [5](#), [6](#), [8](#)
- [42] Tianyu Wang, Xiaowei Hu, Pheng-Ann Heng, and Chi-Wing Fu. Instance shadow detection with a single-stage detector. *IEEE Trans. Pattern Analysis and Machine Intelligence*, 45(3):3259–3273, 2023. [1](#), [2](#), [4](#), [5](#), [6](#), [7](#), [8](#)
- [43] Xinlong Wang, Rufeng Zhang, Tao Kong, Lei Li, and Chunhua Shen. SOLOv2: Dynamic and fast instance segmentation. In *Proc. Advances in Neural Information Processing Systems*, pages 17721–17732, 2020. [2](#)
- [44] Xinlong Wang, Rufeng Zhang, Chunhua Shen, Tao Kong, and Lei Li. SOLO: A simple framework for instance segmentation. *IEEE Trans. Pattern Analysis and Machine Intelligence*, 44(11):8587–8601, 2022. [2](#)
- [45] Zhenghao Xing, Tianyu Wang, Xiaowei Hu, Haoran Wu, Chi-Wing Fu, and Pheng-Ann Heng. Video instance shadow detection under the sun and sky. *IEEE Transactions on Image Processing*, 33:5715–5726, 2024. [1](#)
- [46] Rufeng Zhang, Zhi Tian, Chunhua Shen, Mingyu You, and Youliang Yan. Mask encoding for single shot instance segmentation. In *Proc. IEEE Conf. on Computer Vision and Pattern Recognition*, pages 10223–10232, 2020. [2](#)
- [47] Bolei Zhou, Hang Zhao, Xavier Puig, Sanja Fidler, Adela Barriuso, and Antonio Torralba. Scene parsing through ADE20K dataset. In *Proc. IEEE Conf. on Computer Vision and Pattern Recognition*, pages 5122–5130, 2017. [7](#)
- [48] Bolei Zhou, Hang Zhao, Xavier Puig, Tete Xiao, Sanja Fidler, Adela Barriuso, and Antonio Torralba. Semantic understanding of scenes through the ADE20K dataset. *International Journal of Computer Vision*, 127(3):302–321, 2019. [7](#)
- [49] Xizhou Zhu, Han Hu, Stephen Lin, and Jifeng Dai. Deformable ConvNets V2: More deformable, better results. In *Proc. IEEE Conf. on Computer Vision and Pattern Recognition*, pages 9300–9308, 2019. [3](#)